Synthesis and characterization of Zr-based in situ crystal precipitated and liquid phase separated bulk metallic glass composite

Gyorgy Czel[a], Kinga Tomolya[b], Maria Sveda[b], Anna Sycheva [b], Ferenc Kristaly[c], Andras Roosz[b] Dora Janovszky[b]

[a]Institute of Ceramic and Polymer Engineering, University of Miskolc, Hungary

[b]MTA-ME Materials Science Research Group, Miskolc, Hungary

[c]Institute of Mineralogy and Geology University of Miskolc, Hungary

Keywords: metallic glasses, immiscible alloy, metal matrix composite, mechanical properties, microstructure, fracture

Abstract. The aim of this study was to evaluate new Zr-based bulk metallic composites with crystallized dendrites or droplets which have the volume fraction below the critical one (the percolation limit). The $Cu_{36}Zr_{48}Al_8Ag_8$ alloy was chosen as matrix. Dendrites formed by in-situ solidification due to Ni addition. It was found that a new monotectic alloy system can be created successfully owing to Y addition (1-7 at.%) to the matrix. Small amount of dendrites with non-random distribution has a strong influence on the compressive strength. Experiment showed that the alloy with 4.1 at.% Ni has the maximum compressive strength (1998 MPa) and Young's modulus (86 GPa) within the examined samples. The results of compression test reveal that the cracks propagate near the small droplets below 1 μm in diameter which generate weakening in the microstructure. In contrast, the large droplets especially above 3 μm in diameter create a strong barrier for the shear band propagation.

1. Introduction

Last few years have seen a huge research activity on bulk metallic glasses [1, 2, 3, 4]. Among the metallic systems, the Cu-based bulk metallic glasses (BMGs) have a potential for practical application due to high strength and relatively low material cost [5, 6, 7]. Unfortunately, the BMGs still do not display sufficient ductility for industrial applications. BMGs do not exhibit dislocations to help the forming processes and they have low atomic mobility as well. Deformation takes place only via localized and inhomogeneous shear bands [8, 9]. The plasticity may be improved by secondary ductile phases. Recent studies have indicated that there exists a critical volume fraction of crystalline phases (percolation limit) required to increase the ductility of composites [10-12].

Not only the volume fraction of crystalline phases should be considered, but also another key factor the interphase spacing, the second phase`s shape, size and distribution are also very important parameters affecting mechanical properties [13, 14]. According to some authors the spherical and ductile second phase would be ideal to improve the workability properties owing to the liquid-liquid phase separation [15, 16]. Amorphous or crystalline spherical phase could prevent the crack propagation. However, it has been published that bulk metallic glass-matrix composites (BMGMCs) with in-situ solidified ductile dendrites also can provide larger ductility [17, 18].

In the past decade the deformation of BMGMCs has attracted increasing research interest [19, 20, 21, 22].

The Ag-Cu-Zr system is characterized by a miscibility gap [23, 24]. The homogenous liquid separates into an Ag-rich liquid and a Cu–Zr-rich liquid upon cooling through the miscibility gap. The addition of Y to the ternary system results in separation into Ag-Y-rich liquid and Cu–Zr-rich liquid [25] during cooling in accordance with the highly negative heat of mixing [26] between Ag and Y. The extent of the miscibility gap is extended in the quaternary system. In contrast, the addition of Ni to the ternary system leads to the formation of an Ag-rich and a Cu-Zr-Ni-rich liquids [25] form owing to the highly positive heat of mixing [27] between Ag and Ni. The extent of the miscibility gap does not change due to the Ni addition in the quaternary system.

Bulk glassy samples obtained using conventional cast method with critical diameter exceeding 10 mm have been reported in [28, 29] for Cu-Zr-Ag-Al quaternary system. The critical diameter of a glassy rod is 25 mm for the $Cu_{36}Zr_{48}Al_8Ag_8$ alloy, which exhibits the best glass forming ability (GFA) in this alloy system [30, 31]. The glass transition temperature (T_g) is 417 °C, the supercooled liquid region is equal to 101 °C [31]. It shows high fracture strength of above 1860 MPa, compressive plastic strain of 0.1% and Young's modulus (E) of about 102 GPa [30]. The Vickers hardness has changed from ($HV_{0.2}$) 605 to 688 due to overheating [32]. The compressive fracture strength of this bulk metallic glass has varied from 1252 MPa to 1865 MPa depending on the overheating [32]. Q. Zhang, W. Zhang and co-authors suggest that critical cooling rate of $Cu_{36}Zr_{48}Ag_8Al_8$ alloy is 4.4 K/s and 6.4 K/s or less respectively in two published articles [33, 34]. Both articles refer to the work of Lin et al. who have established a relationship between the critical cooling rates for a number of glass-forming alloys and corresponding maximum dimension. [35].

In the Cu-Zr-Ag-Al system $Cu_{36}Zr_{48}Al_8Ag_8$ alloy has the best GFA. In this composition, we have the opportunity to create in-situ different second phase shapes. Thus, it is obviously worth producing such amorphous/crystalline composites whose composition is close to the composition of $Cu_{36}Zr_{48}Al_8Ag_8$ matrix.

The aim of the present study is two-fold. The first aim is to create BMGMCs whose matrix has same amorphous structure but it is reinforced with different crystalline phases: dendrites or droplets. The second aim is to examine the effect of dendrites or droplets which have the volume fraction below the critical volume fraction (percolation limit) on the mechanical strength. These partly crystallized composites are prepared by in-situ precipitation or liquid-liquid separation due to the addition of Ni or Y and Ni+Y to the Cu-Zr-Ag-Al alloy system. Considering the good bonding between the amorphous matrix and the second phase or phases, the simplest way to produce new type BMGMC is the in-situ phase formation. Hardness measurement and strength evaluation are used for strength characterization; morphology studies support the success of structure developments. The dependences of mechanical properties and microstructures of the in situ BMGMCs on the experimental parameters are summarized below.

2. Experimental procedures

The nominal compositions of the alloys studied in the present work were prepared with the following concept: $Cu_{36}Zr_{48}Ag_8Al_8$ was chosen as base composition. Furthermore, the effect of Y and Ni addition was investigated with varying the alloys with the $(Cu_{36}Zr_{48}Ag_aAl_b)_{100-c-d}Y_cNi_d$ (c= 0-7 at.%, d= 0-7 at.%) formula. Parameters a and b were calculated in order to keep the matrix composition of $Cu_{36}Zr_{48}Ag_8Al_8$ in the CuZrAgAlYNi alloys based on our preliminary experiments. In these experiments the composition of the solidified droplet phases and its volume fraction were measured. These parameters are used to calculate the composition of the average initial composition. The method was established in [24]. The crystalline volume fraction was determined by image analysis, performed on Zeiss Axio Vision Imager equipment using Leica software. The master alloy ingots were prepared by arc-melting from a mixture of pure metals under purified argon atmosphere (min. 99.9 wt.%) with a Ti-getter. The ingots were re-melted by induction melting in a quartz crucible under argon atmosphere. The cast rod was prepared by centrifugal casting with 30 mm in length and 3 mm in diameter under purified argon atmosphere. The cooling rate of our copper mould is estimated on the basis of the secondary dendrite arm spacing [36]. The cooling rate is ~200 K/s and ~1300 K/s at the head (near the top) and the bottom part of the copper mould, respectively. Based on the preliminary experiments, it is expected that a composite can be produced and not a fully amorphous sample using this higher cooling rate. Three cylindrical samples, with a diameter of 3 mm and a height of about 6 mm, were cut from each of as cast rod for uniaxial compression tests. Both ends of the compression samples were polished to be parallel, and minimum six samples were measured for each composition by universal compressive tester equipment. The compression tests were carried out at room temperature in a Zwick/Roell Z250 compression testing machine, with a strain rate of 1.4×10^{-4} s^{-1}. After compression test series, the fracture surfaces were investigated by scanning electron microscopy (SEM).The cross sections of the rod were examined by a Hitachi S-4800 scanning electron microscope (SEM) equipped with BRUKER AXS type energy-dispersive X-ray spectrometer (EDS). Backscattered electron micrographs were recorded in order to get information about the microstructure of the samples. The droplet size distribution was determined by image analysis, performed on Zeiss Axio Vision Imager equipment using Leica software, while the composition of the phases was determined by EDS analysis. The composition of the bulk samples was confirmed by Bruker D8 Advance diffractometer (XRD) using Cu Kα radiation (40 kV, 40 mA), in parallel beam geometry obtained with Göbel mirror, equipped with Vantec-1 position sensitive detector (1° window opening), measured in the 2-100 °(2 θ) angular range, with 0.007° (2 θ)/29 sec speed. The specimen is rotated in sample plane during the measurement, to obtain data from the whole surface and to reduce in plane preferred orientation effects. The crystalline volume fraction was determined by XRD analysis using peak area integration and polynomial background modelling to separate crystalline peaks from amorphous hump (DiffracPlus EVA of Bruker). Additionally, a FEI Tecnai G2 transmission electron microscope equipped with a LaB6 cathode was applied, too. The acceleration voltage was 200 kV. The TEM sample was thinned by ion polishing method (Gatan PIPS)

3. Results and discussion

3.1 Bulk metallic glass composite with dendrites in the Cu-Zr-Ag-Al system

An amorphous/crystalline composite can be produced when the cooling rate is not sufficient for complete amorphisation or the amount of impurity is too high. Unfortunately, the dissolved oxygen is also an undesirable contaminant. In the case of amorphous rods (base material) with different crystalline volume fraction were produced, as demonstrated in Fig. 1. The critical diameters of glassy alloys are greatly influenced by the preparation method. The critical cooling rate for glass formation of $Cu_{36}Zr_{48}Al_8Ag_8$ alloy produced by centrifugal casting is higher than literature value, i.e. higher than ~200 K/s. Precipitated phases could be detected based on the SEM and XRD analyses (Fig. 1a-c). The crystalline volume fraction fluctuated from 7 % to 24 % probably depending on the impurity levels, which promote crystallization. The dendritic morphology suggests that this phase forms first from the liquid and the remaining liquid transforms into amorphous structure at glass transition temperature. Some crystalline diffraction peaks superimposed on a broad amorphous scattering maximum can be seen. TEM-EDS investigation reveals that the chemical composition of this phase is $Cu_{30.4\pm1.8}Zr_{53.9\pm1.5}Ag_{4.3\pm1.0}Al_{11.4\pm0.9}$ at.%. The space group is Fd-3m with cubic structure (a_0=1.217 nm). Based on the indexed diffraction images and the measured chemical composition, this phase's structure is analogous with that of $CuZr_2$. Some Ag atoms substitute the Cu atoms and some Al atoms substitute the Zr atoms; so this unknown phase is $(Ag_{0.14}Cu_{0.86})(Al_{0.19}Zr_{0.81})_2$. Non-random particle distributions have been observed in samples, revealed as a well-developed line pattern.

The Vickers hardness ($HV_{0.01}$) of amorphous structure is 522±14. The Vickers hardness of dendritic phase was not measured because of its small size.

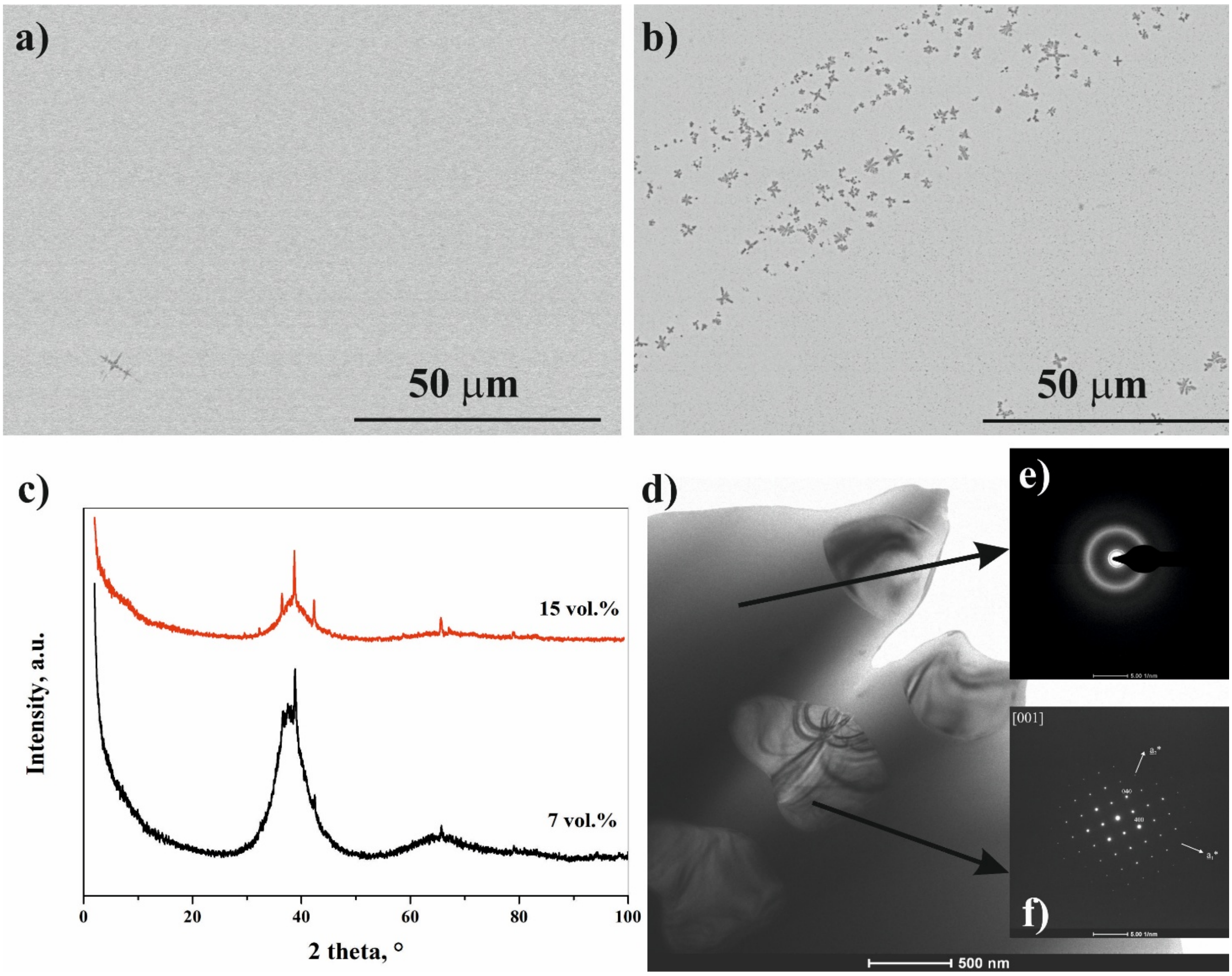

Fig.1: Backscattered SEM micrographs (a, b), XRD patterns of the $Cu_{36}Zr_{48}Al_8Ag_8$ samples with different crystalline volume fraction: a) 7 vol.%, b) 15 vol.% and TEM (d) bright field image of amorphous/crystalline composite the darker unknown phase in the matrix. The inserts in d) represent SAED patterns

3.2 Liquid phase separation in the Cu-Zr-Ag-Al-Y system

Y is one of the favorite minor addition elements for improving the GFA. In our case, the Y addition first of all induces the liquid separation and then improves the GFA. A liquid separation is revealed in the quaternary system as we presented in [37]. Aluminum has negative heat of mixing with all the components of the Cu-Zr-Ag-Y system. In this system with five components cooling the melt beyond a certain limit, causes the homogeneous liquid to separate into an Ag-Y-rich liquid (hereinafter L_1) and a Cu-Zr-rich liquid (hereinafter L_2) by nucleation and growth mechanism in all samples. As Ag-Y rich droplets separate from the liquid, the remaining liquid becomes poor in elemental Ag, so an elevated Ag content of the master alloys is produced (Table 1). The Y content of the $Cu_{35.2}Zr_{45.7}Ag_{10.5}Al_{7.6}Y_1$ master alloy is 1.0 at.%. A well-defined droplet-like structure develops from the Ag-Y rich liquid, which is uniformly distributed in the rod sample of 3 mm diameter. The phase-separated structure can be clearly observed in the SEM images in Fig. 2a. The remaining Cu-Zr rich liquid solidifies into amorphous structures at the T_g temperature based on the XRD measurement (Fig.2b), surrounding the droplets as amorphous matrix. The volume fraction of the separated crystalline phases (drops in BSE images) is about 2 % by XRD. The droplet size is relatively small: the volume fraction of 50.7 % of the particles is below 5×10^{-3} μm^2, the maximum surface area is 25 $\times10^{-3}$ μm^2 (Fig. 2c), namely the droplets diameter is below 180 nm. The average hardness of the sample is approximately $HV_{0.01}$ 540±42.

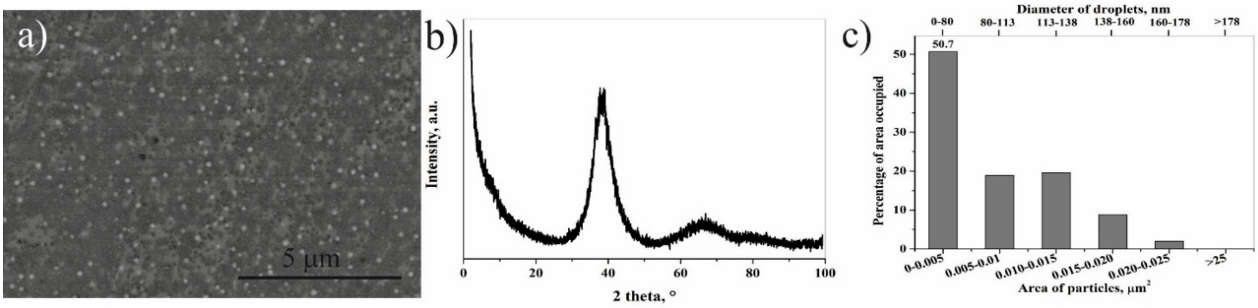

Fig.2: Backscattered SEM micrograph (a), XRD analysis (b), droplet size distribution (c) from the matrix and droplet of the rod sample from $Cu_{35.2}Zr_{45.7}Ag_{10.5}Al_{7.6}Y_{1}$ alloy

The amount of the L_1 droplets can be enhanced by increasing the Y content based on the negative heat of mixing between Ag and Y (Table 1). It can be clearly observed that increasing the amount of Y increases the number of separated droplets (Fig. 3a). Raising the Y content to 4 at.% results in 42 vol.% (measured by XRD)of L_1 phase separated (Fig. 3b), namely multiple times the number of droplets at the Y content of 1 at.%. Observing the size distribution of droplets it can be established that the majority of the droplets is below 1.6 µm in diameter. Nevertheless, 2.7 % of the droplets has surface area between 9 and 10 µm^2 and droplets with a surface area above 100 µm^2 are also detected (Fig. 3c) owing to the coalescence of droplets with increasing the Y content. Different solidified structures can be distinguished in the droplets. During morphology evaluation we could observe with near eutectic inner structure (Fig. 3a - marked as 1). A few *swallow* droplets with distinct structure can be found with distorted structure in which primary phase and eutectic structure have solidified (Fig. 3a - marked as 2). We could also find nano-micro droplets crystallised together with globular droplets (Fig. 3a - marked as 3). Different solidified structures can be distinguished in the droplets. Multiphase microstructure solidified from the huge L_1 liquid drops; a near eutectic structure can be observed (Fig. 3a - marked as 1), but these crystalline droplets have preserved spherical shape. However, a few droplets with distinct structure can be seen, in which primary phase and eutectic structure have solidified and the droplet-like structure is distorted (Fig. 3a - marked as 2). The Vickers hardness ($HV_{0.01}$) of the matrix is 554±32, the hardness of huge L_1 droplets with eutectic structure is 350±16 and with multiphase structure is $HV_{0.01}$ 300±28. The large number of small droplets increases the standard deviation of Vickers hardness of the amorphous structure.

Further increase of the Y content does not lead to obvious increase of the volume fraction of separated Ag-Y- rich droplets. The volume fraction of separated liquid is 18 % in the $Cu_{32.6}Zr_{42.6}Ag_{9.8}Al_{8.0}Y_{7.0}$ alloy (Fig. 4a,b). The liquid separation process has changed considering the structures of the droplets and their size distribution. The diameter of huge droplets does not increase further (Fig, 4c); moreover, a significant increase in the number of small droplets is observed.

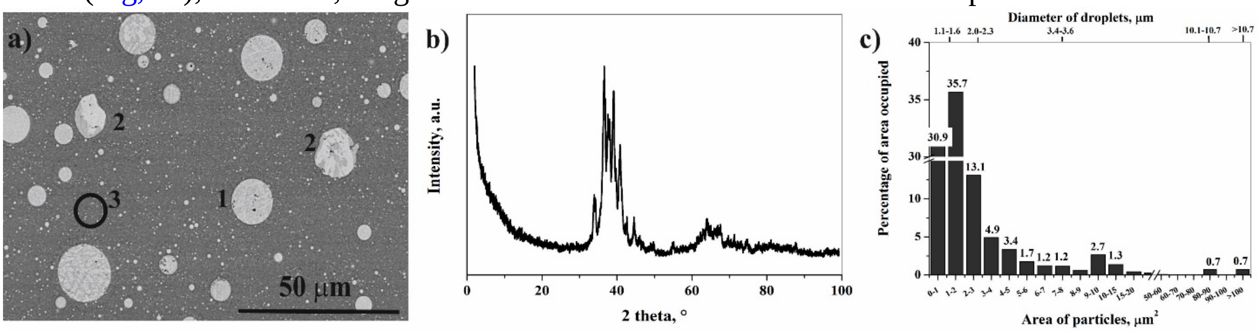

Fig.3: Backscattered SEM micrograph (a) of the matrix and droplets, XRD analysis (b), droplet size distribution (c) of the rod sample from $Cu_{33.9}Zr_{42.4}Ag_{12.4}Al_{7.2}Y_{4.1}$ alloy

Near 50 % of the droplets have a surface area below 0.3 µm^2 and droplets with 1.0-1.5 µm^2 are still present in significant amounts. Pure eutectic structure is not visible in the drops. Two different structures can be realized in the huge droplets: in droplets (generally above 10 µm in diameter) primary phase and eutectic structure (Fig. 4a - marked as 1) are clearly visible. It can be seen that a number of large droplets have lost their spherical shape during solidification: the primary solidified phase has broken through the shell of drop and has grown into the matrix (Fig. 4a-marked as 2) which means that the solidification temperature of droplets is higher than T_g of the amorphous matrix. Small microdroplets with a grain size below 3 μm and volume fraction of 96.3 solidify into phases without internal pattern (Fig. 4d - marked as 3) and do not show any substructure based on the SEM analysis. The hardness of huge spherical droplets is $HV_{0.01}$ 364±20, the hardness of non-spherical droplets is $HV_{0.01}$ 303±7, the average hardness of matrix is $HV_{0.01}$ 504±73.

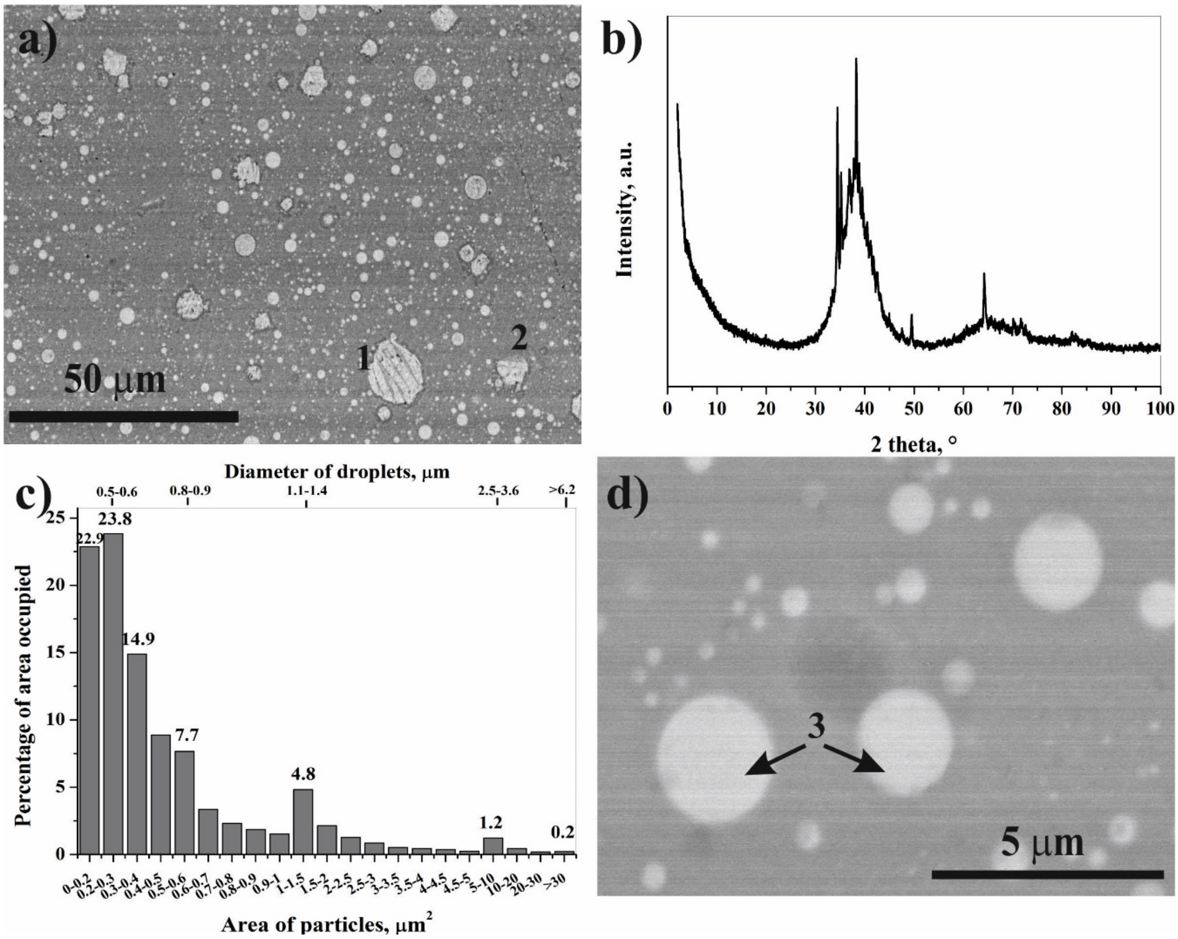

Fig.4: Backscattered SEM micrograph (a), XRD analysis (b), droplet size distribution (c) and SEM micrograph of droplet with one phase (d) of the rod sample from $Cu_{32.6}Zr_{42.6}Ag_{9.8}Al_{8.0}Y_{7.0}$ alloy

3.3 Bulk metallic glass composites with crystalline phases in the Cu-Zr-Ag-Al-Ni system

Nickel has negative heat of mixing with all the components of the Cu-Zr-Al system [26,27]; conversely, heat of mixing between Ni and Ag is positive, which creates a monotectic system. Liquid separation does not take place due to the Ni addition to the $Cu_{36}Zr_{48}Al_8Ag_8$ alloy, furthermore Al-Cu-Zr-rich dendritic phase (Fig. 5a - marked as 1) formed island-like and blended during cooling in the $Cu_{35,6}Zr_{47,6}Ag_{7,9}Al_{7,9}Ni_1$ rod-shape sample. The volume fraction of crystalline phase is 35 %. The hardness of amorphous matrix is $HV_{0.01}$ 516±22.

The dendrites contain Al so an elevated Al content of master alloys were produced hereinafter. A new phase with cauliflower-like morphology (Fig.6a marked as 2) appears beside the dendrites (Fig.6a - marked as 1), owing to further Ni addition to the $Cu_{33.7}Zr_{46.0}Ag_{7.2}Al_{8.9}Ni_{4.1}$ sample. The volume fraction of crystalline phase is reduced to 11 % measured by XRD which means that the glass forming ability increases owing to 4.1 at.% Ni addition. This phenomenon is in accordance with literature; whereby the intermediate transition metal atoms of Fe, Co, Ni have improved the GFA when the amount exceeds a certain limit [38]. The chemical composition of dendrites is

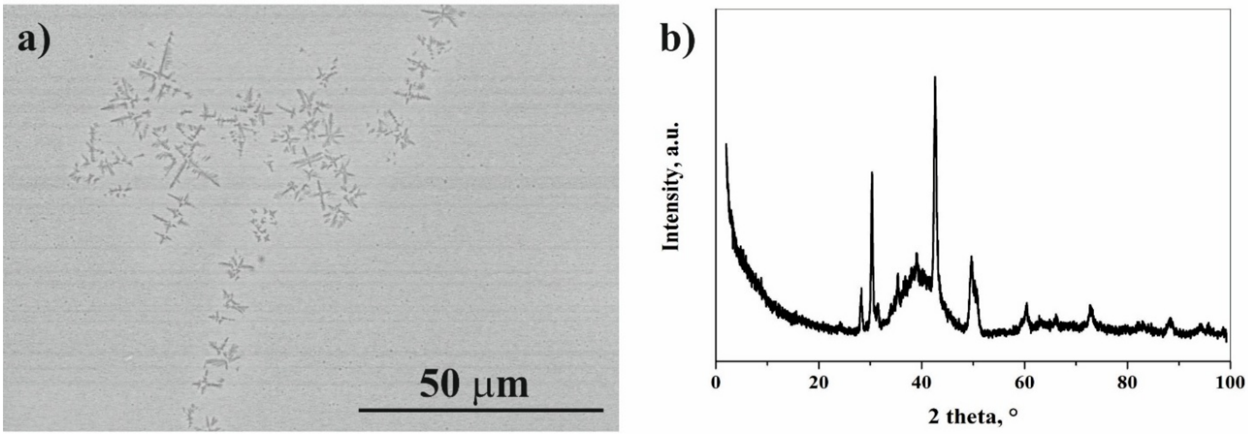

Fig.5: (a,) Backscattered SEM micrographs and (b) diffraction patterns of the $Cu_{35.6}Zr_{47.6}Ag_{7.9}Al_{7.9}Ni_1$ as cast rod sample with 3 mm diameter

$Cu_{29.3}Zr_{49.9}Ag_{2.6}Al_{15.7}Ni_{2.5}$ based on the TEM-EDS investigation. The space group is Fd-3m with cubic structure (a_0=1.217 nm). Comparing the composition of dendrites in $Cu_{36}Zr_{48}Al_8Ag_8$ alloy it can be established that the presence of Ni results in the formation of dendrites, similarly to the base alloy. However, these dendrites dissolve some Ni. The composition of the phase with cauliflower-like morphology is $Cu_{35}Zr_{47}Ag_7Al_4Ni_7$. The matrix composition is $Cu_{37}Zr_{44}Ag_7Al_7Ni_4$, i.e. the composition of the phase with cauliflower-like morphology slightly differs from that of the matrix. Based on the SEM analysis, the liquid separation did not occur in the samples upon addition of 1 and 4.1 at.% of Ni. The hardness of amorphous matrix is $HV_{0.01}$ 552±8. The addition of 7 at.% Ni does not result in amorphous structure.

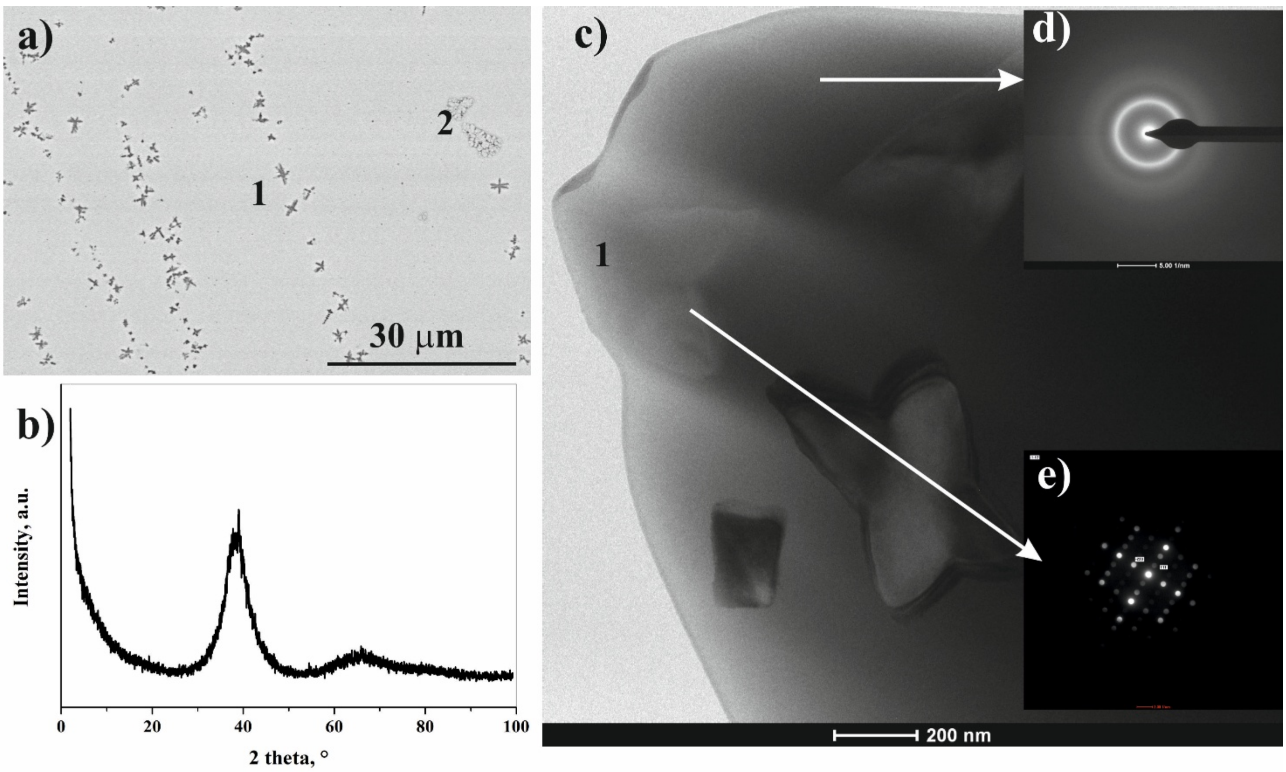

Fig.6: (a) Backscattered SEM micrographs, (b) diffraction pattern of $Cu_{33.7}Zr_{46.0}Ag_{7.2}Al_{8.9}Ni_{4.1}$ as cast rod sample with 3 mm diameter and TEM (c) bright field image of amorphous/crystalline composite. The inserts in c) represent SAED patterns

3.4 Bulk metallic glass composites produced by liquid separation in the Cu-Zr-Ag-Al-Y-Ni system

Owing to the Y and Ni combined addition liquid separation can be revealed in the $Cu_{32.4}Zr_{43.2}Ag_{7.2}Al_{7.2}Y_5Ni_5$ sample (Fig. 7a), primary dendrites do not solidify. The matrix has amorphous structure based on XRD analysis (Fig. 7b) and the composition is $Cu_{35.4}Zr_{50.3}Ag_{2.1}Al_{6.7}Y_{0.1}Ni_{5.3}$ according to EDS. The crystalline volume fraction is 16 % based on the XRD analysis. In this system, the droplet size distribution shows that vast majority of the droplets is below 1 μm in diameter- *nano-micro droplets* (Fig. 7c), while 6.4 % of the droplets is above 3 μm in diameter. In this sample two different structures can be observed in the droplets above 1 μm in diameter; some (generally) larger droplets have multiphase structure (Fig.7- marked as 1), but there are droplets solidifying into one phase with a maximum diameter of 10 μm (Fig.7 -marked as 2). The hardness of droplets with single phase structure is $HV_{0.025}$ 416±60 and of those with multiphase structure is $HV_{0.01}$ 258±25. The difference is too large indicating different structure of phases in solidified droplets. The hardness of matrix is $HV_{0.01}$ 495±11.

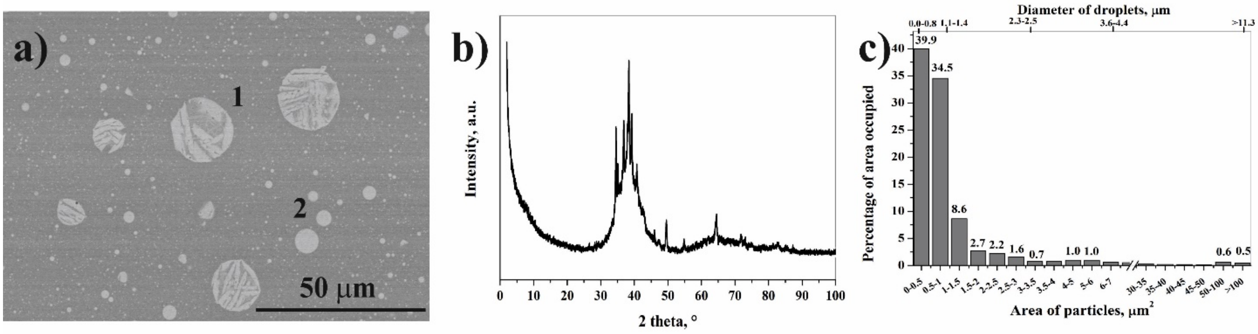

Fig.7: Backscattered SEM micrographs (a), XRD analysis (b) and droplet size distribution (c) of the rod sample from $Cu_{32.4}Zr_{43.2}Ag_{7.2}Al_{7.2}Y_5Ni_5$ alloy

3.5 Mechanical properties and fracture surfaces

Three D3x6 mm sized compression test samples were cut from all cylindrical cast rods. The crystalline volume fraction and hardness were measured along the longitudinal section of the rod showing slightly varying crystalline volume fraction and hardness along the length (Fig.8a). The melt of BMGMCs follows the flow properties of Newtonian liquids. One can see the flow lines in the longitudinal section of a $Cu_{36}Zr_{48}Al_8Ag_8$ rod. Developed dendrites are situated along the flow lines, and behave themselves as flow line tracers. In the case of samples with liquid-liquid separation we could observe a similar flow line effect (Fig.8b) due to small micro droplets. Generally the sample cut from near the top has the highest compressive strength.

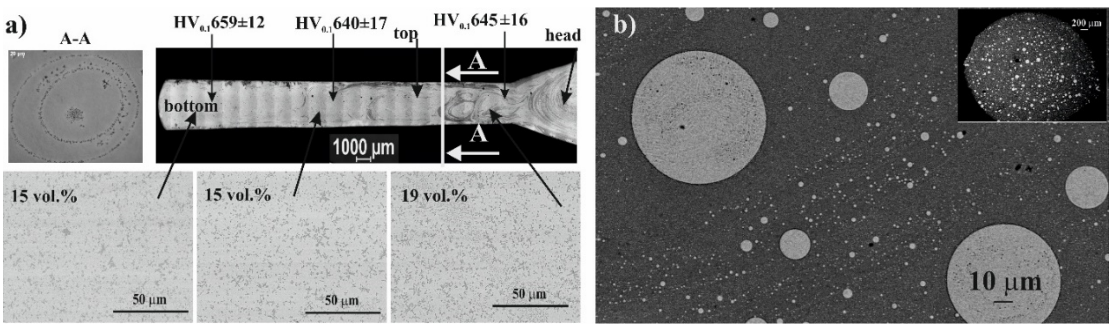

Fig.8: Optical and backscattered SEM micrographs, Vickers hardness and crystalline volume fraction along the longitudinal section of $Cu_{36}Zr_{48}Al_8Ag_8$ rod (a), backscattered SEM micrographs of cross section of $Cu_{33.9}Zr_{42.4}Ag_{12.4}Al_{7.2}Y_{4.1}$ rod (b)

Table 1

Mechanical properties under compressive loading and estimated crystalline volume fraction for each tested sample and for the literature. The crystalline volume fractions were obtained from XRD analysis

Nominal compositions at.%	Estimated cryst. vol. fraction, vol.% by XRD	σ_f, MPa		Young's modulus, GPa	Max. strain, %	Energy to break at the top, xE7, J/m³
		top	middle			
$Cu_{36}Zr_{48}Al_8Ag_8$*	0	1589±236		105	2.0	-
$Cu_{36}Zr_{48}Al_8Ag_8$	7	1582±104	1443±87	78±5	2.01	2.74±0.18
$Cu_{36}Zr_{48}Al_8Ag_8$	15	1423±20	1297±47	72±2	1.91	2.60±0.04
$Cu_{36}Zr_{48}Al_8Ag_8$	17	1667±35	1630±41	77±0.7	1.98	2.91±0.68
$Cu_{36}Zr_{48}Al_8Ag_8$	20	1435±50	1429±70	73±4	1.91	2.78±0.17
$Cu_{36}Zr_{48}Al_8Ag_8$	24	1739±68	1693±79	76±2	2.16	3.47±0.64
$Cu_{35.2}Zr_{45.7}Ag_{10.5}Al_{7.6}Y_1$	2	1640±128	1458±263	74±4	2.14	3.37±0.62
$Cu_{33,9}Zr_{42,4}Ag_{12,4}Al_{7,2}Y_{4,1}$	42	1405±15	1362±30	74±4	1.85	2.50±0.27
$Cu_{32.6}Zr_{42.6}Ag_{9.8}Al_{8.0}Y_{7.0}$	18	1266±63	1013±46	64±9	1.89	2.16±0.03
$Cu_{35,6}Zr_{47,6}Ag_{7,9}Al_{7,9}Ni_1$	35	1586±421	1511±221	76±1	2.29	2.73±0.91
$Cu_{33.7}Zr_{46.0}Ag_{7.2}Al_{8.9}Ni_{4.1}$	11	1723±274	1525±28	86±9	1.94	2.97±0.24
$Cu_{33.5}Zr_{44.7}Ag_{7.4}Al_{7.4}Ni_{7.0}$	100	-		-	-	-
$Cu_{32.4}Zr_{43.2}Ag_{7.2}Al_{7.2}Y_5Ni_5$	16	1493±168	1430±170	66±4	2.22	3.30±0.59

The ultimate compressive fracture strength and Young's modulus are generally within the range of standard deviance of fully amorphous sample published in literature (Fig. 9a, Table 1). The mechanical properties strongly depend on the volume fraction, distribution and type of crystalline phases (Fig. 9). The standard deviation of the ultimate compressive fracture strength is large; however, the matrix material is sensitive to overheating [32] and the casting process might cause defects like pores in the sample.

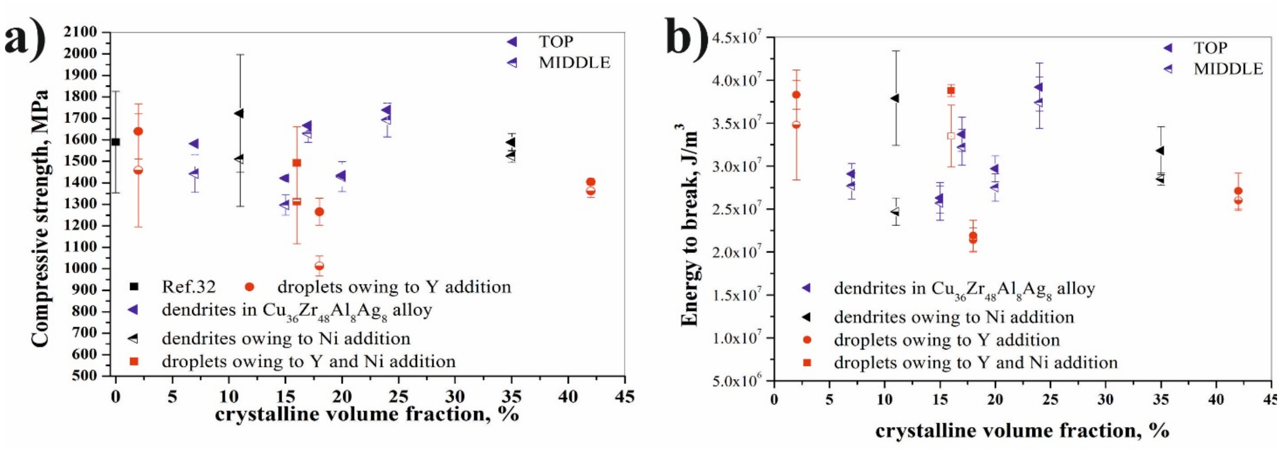

Fig.9: The maximum engineering compressive fracture strength (a) and energy to break (b) as function of crystalline volume fraction (measured by XRD)

The specific energy to break is the energy required to cause material failure and may be determined by integration of the stress–strain curve (Fig. 9b). The dendrites do not significant decrease in compressive stress in the case of Ni addition and base alloy with 24 vol.% dendrite.

The compressive stress–strain curves of $Cu_{36}Zr_{48}Al_8Ag_8$ rod series with diameters of 3 mm can be seen in Figure 10a, c. These samples contain in-situ solidified dendrites with non-random distributions within the glass matrix.

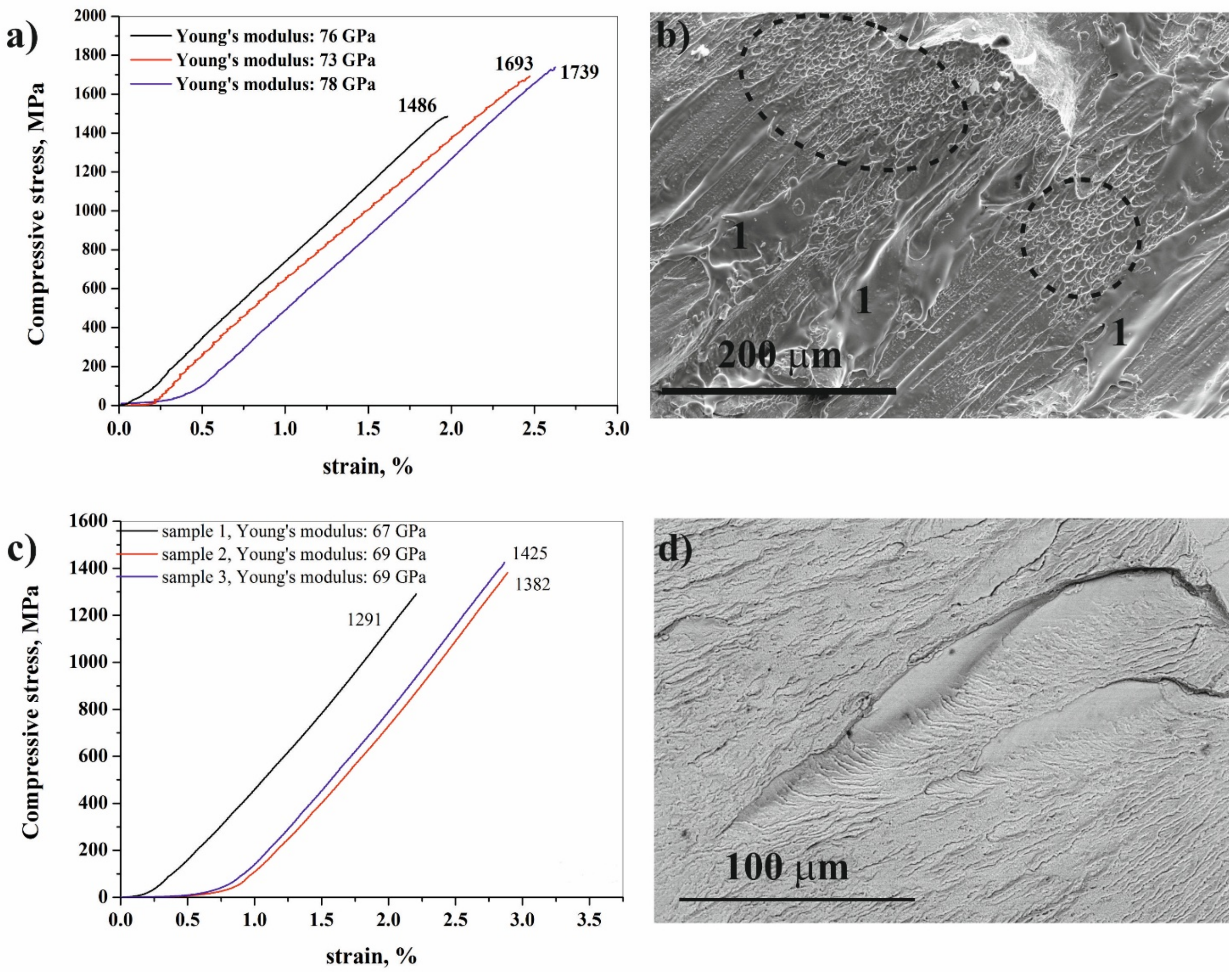

Fig.10: Engineering compressive stress–strain curves (a, c) of the $Cu_{36}Zr_{48}Al_8Ag_8$ samples with different crystalline volume fraction and SEM images (b, d) of fracture surfaces show a vein-like structure (circle) and resolidified material (1); a, b: volume fraction of dendrites 17 %, c, d: volume fraction of dendrites 7 % ; blue line: sample from the top, red line: sample from the middle, black line: sample from the bottom

Generally the ductility depends on the interdendrite spacing and volume fraction [13, 14]. In our case the interdendrite spacing is too large, while the volume fraction of the dendrite is small (max. 24 vol.%); due to this phenomenon, the fine dendrites cannot retard the propagation of shear bands. The dendrites can increase the fracture strength and Young's modulus despite of non-random particle distribution (Fig. 10, Table 1).

The average Young's modulus varies in the range 72 GPa to 78 GPa. The break energy increases with increasing the crystalline volume fraction. The fracture morphology consists of four different areas: a vein-like pattern (marked by circle in Fig. 10b), intermittent smooth regions, multiple shear bands and river-like pattern (Fig. 10d). The vein-like pattern is more pronounced in the larger plastic strain. In the case of 17 vol.% crystalline phases it can be seen a little plasticity. In multiple shear bands initiated from vein-like pattern (marked with dotted circles in Fig.10) and resolidified material appears (marked as 1 in Fig. 10b), which suggests that localized melting might have occurred during the final failure event. The fracture surface of the sample with 7 vol.% dendrite displays a fracture surface with river-like pattern.

An obvious trend has been observed with respect to the Y content, i.e. crystalline droplet size and volume fraction in terms of microstructure and mechanical properties in series Y content alloys (Fig. 11). The ultimate compressive fracture strength and energy to break (Table 1) decrease due to increasing volume fraction of crystalline droplets; although, this decrease is not as great as in the case of dendrites in the $Cu_{36}Zr_{48}Al_8Ag_8$ samples. The morphology of the fracture surface changes depending on the alloy composition with different Y addition.

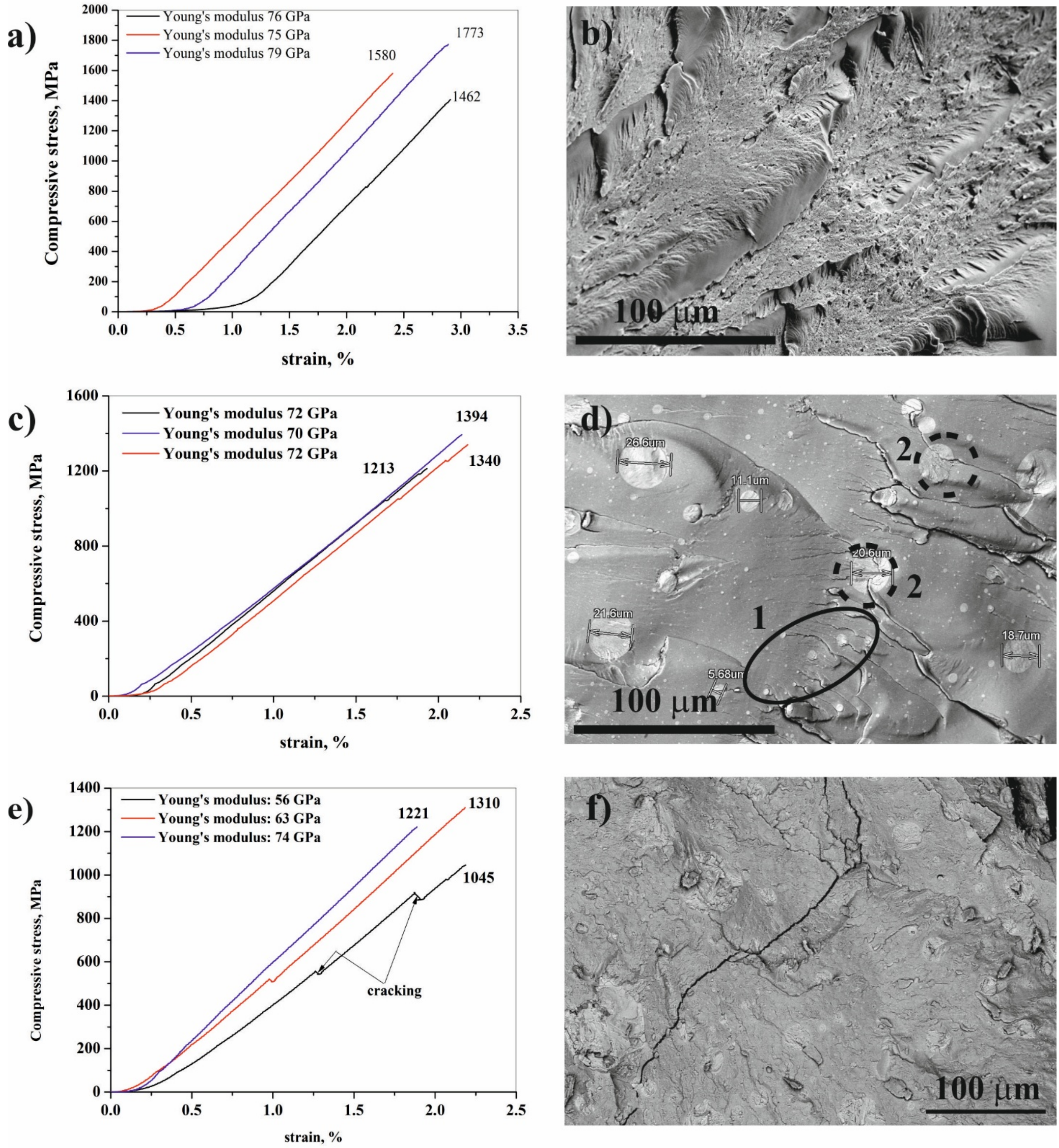

Fig.11: Engineering compressive stress–strain curves (a, c, e) and SEM images of the fracture surfaces (b, d, f) of different Y content alloys with a diameter of 3 mm: a-b) $Cu_{35.2}Zr_{45.7}Ag_{10.5}Al_{7.6}Y_1$, c-d) $Cu_{33.9}Zr_{42.4}Ag_{12.4}Al_{7.2}Y_{4.1}$, e-f) $Cu_{32.6}Zr_{42.6}Ag_{9.8}Al_{8.0}Y_{7.0}$ samples; blue line: sample from the top, red line: sample from the middle, black line: sample from the bottom section

Apparently, the ductility does not appear when droplets of maximum ~180 nm in diameter are in amorphous matrix owing to the 1 at.% Y addition. Under compression, shear bands initiate and propagate, since these droplets do not act as a barrier in the amorphous matrix. These rods suffer from sudden brittle failure. It has been found that the maximum compressive fracture strength (1604±125 MPa) and Young's modulus (74±4 GPa) slightly decrease owing to the 1 at.% Y addition (Fig. 11a, Table 1). The energy to break is 3.37E7 J/m^3. The fracture surface displays dimples in river-like ones and smooth regions of almost zero ductility (Fig. 11b).

An increase in the volume fraction of the crystalline phase leads to an increase in the drop size since the coagulation of little droplets occurs. As a result, the ultimate compressive fracture strength (1354 MPa) and Yield's strength also decrease (Fig. 11c, Table 1) due to the 4.1 at.% Y addition. This Y alloying causes a 25% decrease in the energy to break (2.50E7 J/m^3). A significant change can be observed in the fracture surface. No vein-like or river-like areas are revealed, but the surface exhibits smooth regions and a number of Ag-Y-rich spheres. Both Ag-Y-rich droplets (near eutectic structure and multiphase structure) have smaller hardness ($HV_{0.01}$ 350 and 300 respectively) than the amorphous matrix ($HV_{0.01}$ 527). A large number of fine non-propagating cracks in the Cu-Zr-rich glassy matrix are in contact with the Ag-Y-rich particles of grain size below 3 μm which are 90 vol.% of the droplets (marked as circle '1' in Fig. 11d). The cracks propagating in the matrix change their direction crossing through the big Ag-Y-rich spheres (marked as circle '2' in Fig. 11d), which have a near eutectic structure.

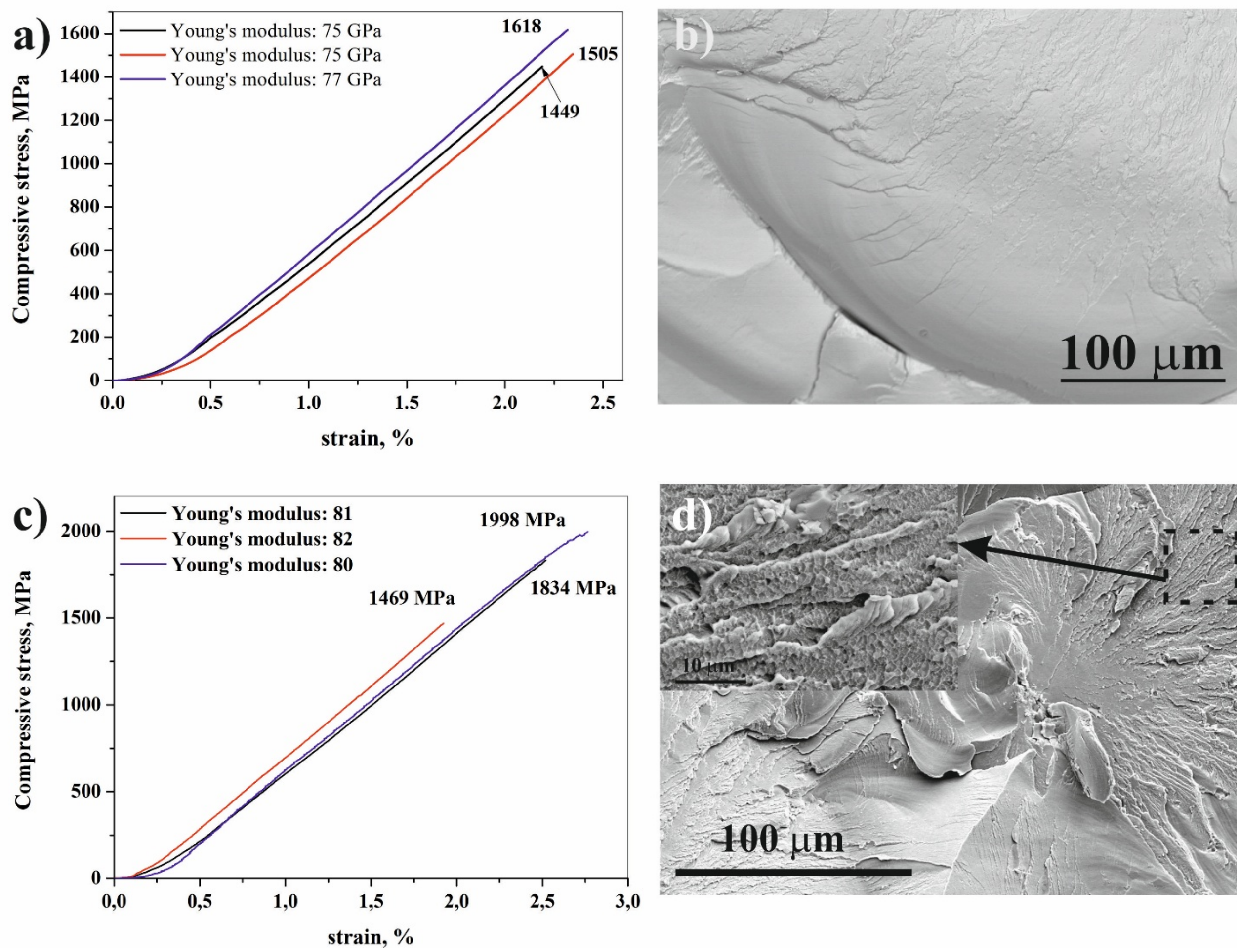

Fig.12: Engineering compressive stress–strain curves (a,c) and SEM images of the fracture surface (b,d) of different Ni content alloys with a diameter of 3 mm: a-b) $Cu_{35.6}Zr_{47.6}Ag_{7.9}Al_{7.9}Ni_1$, c-d) $Cu_{33.7}Zr_{46.0}Ag_{7.2}Al_{8.9}Ni_{4.1}$; blue line: sample from the top, red line: sample from the middle, black line: sample from the bottom section

In the case of 7 at.% Y content the ultimate compressive fracture strength, Young's modulus and the energy to break values continue to decrease (Fig. 9). Cracking is clearly visible in the stress-strain curves (Fig. 11e). The samples collapse discontinuously. In these samples, the drops below 1 μm in diameter are the vast majority (~84 vol.%) and cracks pass along the small droplets (Fig. 11f). The propagating cracks change their direction owing to the big drops (bypass the barriers wriggly) or the big drops prevent the shear bands from rapid propagation. The fracture surface is rough.

Considering the Ni addition it can be established that the ultimate compressive strength (max.1998 MPa) and Young's modulus (86 GPa) are the highest among the examined samples owing to the 4.1 at.% Ni addition. The average strength is 1723 MPa with greater scatter (±274) (Fig. 11a, Table 1). The energy to break is 2.97E7 J/m^3. Although the plastic strain is still very low (0.1 %), the fracture surface exhibits quite different morphology, consisting of smooth regions and river-like patterns (Fig. 11b).

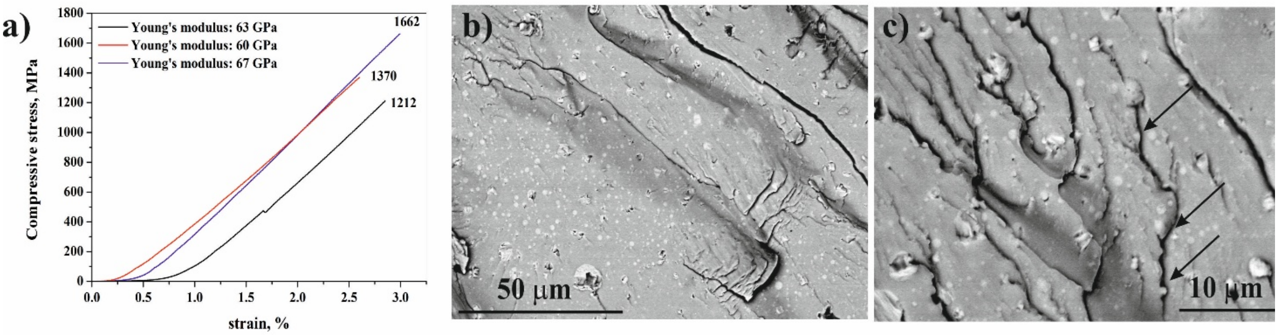

Fig.13: Compressive stress–strain curves (a) and SEM images of the fracture surface (b,c) of the $Cu_{32.4}Zr_{43.2}Ag_{7.2}Al_{7.2}Y_5Ni_5$ as cast rod sample of 3 mm diameter; blue line: sample from the top, red line: sample from the middle, black line: sample from the bottom section

Due to the Y and Ni combined alloying, the compressive stress and Young's modulus fall within the row of Y addition series (Fig. 8). The standard deviation is greater than in the case of only Y addition (Table 1). The strain at failure (2.22 %) and the energy to break (3.30 J/m^3) are higher than in the case of Y or Ni addition. It is likely that the Ag-Y-rich crystallized spheres from 0.2 μm to 1.4 μm in size are governing parts of cracking upon loading. The cracks pass beside the small drops as a yarn necklace (Fig.13b, c). It implies that small droplets below 1 μm in diameter generate weakening of the microstructure. Conversely, big drops (larger than 3 μm in size) block the shear bands or deflect the progression of cracks. Half of the samples collapsed discontinuously, cracking is clearly observed in the stress-strain curves.

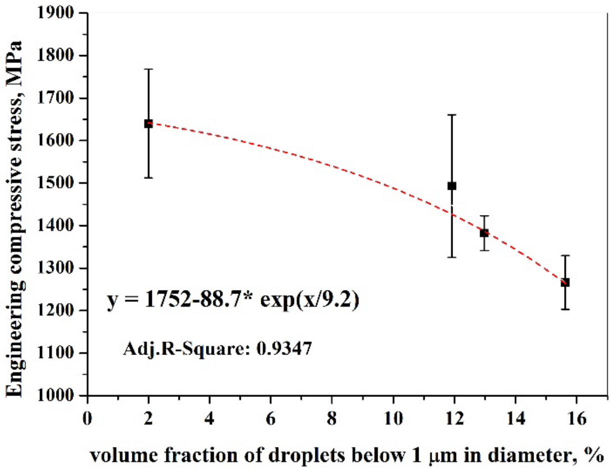

Fig.14: Correlation (best fit function) between the volume fraction of droplets below 1 μm in diameter and engineering compressive stress (from the top section of rod)

Regarding the strains, it can be concluded that the volume fractions of different phases are below the critical volume fraction required to cross brittle-ductile transition. In the case of dendrites, the 42 V/V% is below the percolation limit and 35 V/V% for droplets. However, it is interesting to know how the different phases affect the mechanical properties. The morphology of droplets and dendrites is different. On this basis, one would expect that the mechanical properties are better in the case of composites containing droplets. Comparing the effect of dendrites and droplets in these alloy systems it can be established that the dendrites are favourable considering the mechanical properties however it should be noted that the trend are close to the standard deviations. The strength of the composites does not follow the rule of mixtures or the load bearing model [39] in the base alloy with dendrites (Fig.9). The droplets can prevent the crack propagation if coagulation occurs in exceptionally swift manner and the average droplet size is above 3 μm in diameter.

Droplets smaller than 1 μm in diameter are not an obstacle to block cracks for this reason it is necessary separate effect of the two different droplet sizes. It can be established that increasing the volume fraction of droplets below 1 μm in diameter the engineering compressive stress decreases (Fig.14).

4. Conclusions

The microstructure and mechanical properties of Zr–based bulk metallic glass composites with in situ precipitated crystals or liquid phase separation were investigated. The following conclusions have been drawn from the presented study:

1. New bulk metallic composites can be created with appropriately chosen alloying elements whose matrix has same amorphous structure but it is reinforced with different crystalline phases: dendrites or droplets.
2. Ag-Y rich droplets develop during liquid phase separation owing the Y or Y and Ni combined addition to the $Cu_{36}Zr_{46}Al_{10}Ag_8$ alloy.
3. Mechanical properties are strongly influenced by droplets below 1 μm in diameter. A strong correlation has been found between the engineering compressive stress and volume fraction of droplets smaller than 1 μm in diameter. The cracks pass beside the small drops as a yarn necklace, small drops (below 1 μm in diameter) act essentially as dislocations in traditional crystalline materials. Conversely, big drops (especially above 3 μm in size) block the shear bands or deflect the progression of cracks.
4. Liquid separation does not take place due to the addition of 1-7 at.% Ni to the $Cu_{36}Zr_{46}Al_{10}Ag_8$ alloy, dendrites solidify in the amorphous matrix.
5. The maximum compressive fracture strength, break energy and Young's modulus are the highest among the examined samples owing to the 4.1 at.% Ni addition.

Acknowledgement

The authors wish to thank FemAlk Zrt. (Budapest) for cutting of examined rods by spark erosion.

References

[1] A. Inoue, Stabilization of metallic supercooled liquid and bulk amorphous alloys, Acta Mater. 48 (2000) 279-306.

[2] G. Wang, H.B. Fan, Y.J. Huang, J. Shen, Z.H. Chen, A new TiCuHfSi bulk metallic glass with potential for biomedical applications Chen, Mater Des. 54 (2014) 251-255.

[3] J. Wu, Y. Pan, X. Li, X. Wang, Designing plastic Cu-based bulk metallic glass via minor addition

of nickel, Mater Des. 57 (2014) 175-179.
[4] D.V. Louzguine-Luzgin, Bulk Metallic Glasses and Glassy/Crystalline. In: Novel Functional Magnetic Materials: Fundamentals and Applications, Springer Series in Materials Science 231, Switzerland, 2016 pp. 397-440.
[5] W. Zhou, J. Hou, Z. Zhong, J. Li, Effect of Ag content on thermal stability and crystallization behavior of Zr–Cu–Ni–Al–Ag bulk metallic glass, J. Non-Cryst. Solids. 411 (2015) 132-136.
[6] W. Zhou, J. Hou, W. Weng, Microstructure, thermal stability and mechanical properties of Zr–Cu–Al–Sn bulk metallic glass, J. Non-Cryst. Solids. 429 (2015) 208-212.
[7] Q.P. Cao, J.B. Jin, Y. Ma, X.Z. Cao, B.Y. Wang, S.X. Qu, X.D. Wang, D.X. Zhang, J.Z. Jiang, Enhanced plasticity in Zr-Cu-Ag-Al-Be bulk metallic glasses, J. Non-Cryst. Solids 412 (2015) 35-40.
[8] I. Binkowski, G.P. Shrivastav, J. Horbach, S.V. Divinski, G. Wilde, Shear band relaxation in a deformed bulk metallic glass, Acta Mater. 109 (2016) 330-340.
[9] C.A. Schuh, T.C. Hufnagel, U. Ramamurty, Mechanical behavior of amorphous alloys, Acta Mater. 55 (2007) 4067-4109.
[10] Z.Q. Liu, G. Liu, R.T. Qu, Z.F. Zhang, S.J. Wu, T. Zhang, Microstructural percolation assisted breakthrough of trade-off between strength and ductility in CuZr-based metallic glass composites, Scr. Rep. 4 (2014) 4167.
[11] J. Qiao, H. Jia, P. K. Liaw, Metallic glass matrix composites, Mat. Sci. Eng. R 100 (2016) 1-69.
[12] S. H. Hong, J. T. Kim, M. W. Lee, J. M. Park, M. H. Lee, B. S. Kim, J. Y. Park, Y. Seo, J. Y. Suh, P. Yu, M. Qian, K. B. Kim, Phase Transformation and Work-hardening Behavior of Ti-based Bulk Metallic GLASS Composite, Applied Microscopy 45 (2015) 37-43.
[13] J. Bai, J.S. Li, J. Wang, H.C. Kou, P.K. Liaw, Temperature dependent dynamic flow behavior of an in-situ Ti-based bulk metallic glass composite, Mater. Sci. Eng. A 627 (2015) 21-26.
[14] C.N. Kuo, J.C. Huang, X.H. Du, X.J. Liu, T.G. Nieh, Comparison of mechanical response in CuZrAl–V and CuZrAl–Co bulk metallic glass composites, J. Alloys Compd. 586 (2014) S14-S19.
[15] J. He, N. Mattern, J. Tan, J.Z. Zhao, I. Kaban, Z. Wang, L. Ratke, D.H. Kim, W.T. Kim, J. Eckert, A bridge from monotectic alloys to liquid-phase-separated bulk metallic glasses: Design, microstructure and phase evolution, Acta Mater 61 (2013) 2102-2112.
[16] J.H. Han, N. Mattern, B. Schwarz, S. Gorantla, T. Gemming, J. Eckert, Microstructure and magnetic properties of Gd-Hf-Co-Al phase separated metallic glasses, Intermetallics 20 (2012) 115-122.
[17] P. Gargarella, S. Pauly, M. S. Khoshkhoo, U. Kühn, J. Eckert, Phase formation and mechanical properties of Ti–Cu–Ni–Zr bulk metallic glass composites, Acta Mater. 65 (2014) 259-269.
[18] Y.S. Wang, G.J. Hao, J.W. Qiao, Y. Zhang, J.P. Lin, High strain rate compressive behavior of Ti-based metallic glass matrix composites, Intermetallics 52 (2014) 138-143.
[19] Z. Chu, G. Yuan, H. Kato, G. Xie, D. Yan, The study on interface and property of TiNb/Zr-based metallic. glassy composite fabricated by SPS, J. Non-Cryst. Solids 426 (2015) 83-87.
[20] JA. Kolodziejska, H. Kozachkov, K. Kranjc, A. Hunter, E. Marquis, W.L. Johnson, K.M. Flores, D.C. Hofmann, Towards an understanding of tensile deformation in Ti-based bulk metallic glass matrix composites with BCC dendrites, Scientific Reports 6 (2016) 22563, 1-8.
[21] W. Li, H. Bei, Y. Gao, Effects of geometric factors and shear band patterns on notch sensitivity in bulk metallic glasses, Intermetallics 79 (2016) 12-19.
[22] X. Xu, N. Li, L. Liu, Intrinsic or extrinsic size-dependent deformation behavior of a Zr-based bulk metallic glass in supercooled liquid state?, J. Alloys Compd. 589 (2014) 524-530.
[23] A. Castellero, D.H. Kang, I.H. Jung, G. Angella, M. Vedani, M. Baricco, Rapid solidification of silver-rich Ag–Cu–Zr alloys, J. Alloys Compd. 536 (2012) S148-S153.
[24] D. Janovszky, K. Tomolya, A. Sycheva, G. Kaptay, Stable miscibility gap in liquid Cu–Zr–Ag ternary alloy, J. Alloys Compd. 541 (2012) 353-358.

[25] D. Janovszky, K. Tomolya, M. Sveda, A. Sycheva, G. Kaptay, Effect of Y and Ni addition on liquid immiscibility in Cu–Zr–Ag ternary alloys, J. Alloys Compd. 615 (2014) S616-S620.
[26] S.V. Ketov, L.V. Louzguina-Luzgina, A.Y. Churyumov, A.N. Solonin, D.B. Miracle, D.V. Louzguine-Luzgin, A.Inoue, Glass-formation and crystallization processes in Ag–Y–Cu alloys, J. Non-Cryst. Solids 358 (2012) 1759-1763.
[27] U. Saeed, H. Flandorfer, H. Ipser, Lead-free solders: Enthalpies of mixing of liquid Ag–Cu–Ni–Sn alloys, J. Mater.Res. 21 (2006) 1294-1304.
[28] Y.C. Kim, J.C. Lee, P.R. Cha, J.P. Ahn, E. Fleury, Enhanced glass forming ability and mechanical properties of new Cu-based bulk metallic glasses, Mater. Sci. Eng. A 437 (2006) 248-253.
[29] Q. Zhang, W. Zhang, G. Xie, A. Inoue, Glass-Forming Ability and Mechanical Properties of the Ternary Cu-Zr-Al and Quaternary Cu-Zr-Al-Ag Bulk Metallic Glasses, Mat. Trans. 48 (2007) 1626-1630.
[30] W. Zhang, Q. Zhang, A. Inoue, Formation and thermal stability of new Zr–Cu-based bulk glassy alloys with unusual glass-forming ability, J. Alloys Compd. 483 (2009) 112-115.
[31] Q.S. Zhang, W. Zhang, DV. Louzguine-Luzgin, A. Inoue, Effect of substituting elements on glass-forming ability of the new Zr48Cu36Al8Ag8 bulk metallic glass-forming alloy, J. Alloys Compd. 504S (2010) S18-S21.
[32] Y. Zhao, S. Kou, H. Suo, R. Wang, Y. Ding, Overheating effects on thermal stability and mechanical properties of Cu36Zr48Ag8Al8 bulk metallic glass, Mater Des. 31 (2010) 1029-1031.
[33] Q. Zhang, W. Zhang, A. Inoue, New Cu–Zr-based bulk metallic glasses with large diameters of up to 1.5 cm, Scripta Mater. 55 (2006) 711-713.
[34] W. Zhang, Q. Zhang, A. Inoue, Fabrication of Cu-Zr-Ag-Al glassy alloy samples with a diameter of 20 mm by water quenching, J. Mater. Res. 23 (2008) 1452-1456.
[35] X.H. Lin, W.L. Johnson, Formation of Ti–Zr–Cu–Ni bulk metallic glasses, J. Appl. Phys. 78 (1995) 6514-6519.
[36] B. A. Richardson, D.H. Kirkwood, Proc. Conf. on Solidification and Cast of Metals, Metals Society London (1979) 44-52.
[37] D. Janovszky, K. Tomolya, Designing amorphous/crystalline composites by liquid-liquid phase separation, Mat. Sci Forum 790-791 (2014) 473-478.
[38] W. H. Wang, Roles of minor additions in formation and properties of bulk metallic glasses, Prog. Mat. Science 52 (2007) 540–596.
[39] S. Pauly, G. Liu, G. Wang, U. Kühn, N. Mattern, J. Eckert, Microstructural heterogeneities governing the deformation of Cu47.5Zr47.5Al5 bulk metallic glass composites, Acta Mater. 57 (2009) 5445-5453.